coatings

MDPI

Communication

Characterization of $Cd_xTe_yO_z$/CdS/ZnO Heterostructures Synthesized by the SILAR Method

Yana Suchikova [1,*], Sergii Kovachov [1], Ihor Bohdanov [1], Elena Popova [2], Aleksandra Moskina [3] and Anatoli Popov [3]

[1] The Department of Physics and Methods of Teaching Physics, Berdyansk State Pedagogical University, 71100 Berdyansk, Ukraine
[2] Centro de Investigación en Astronomía, Universidad Bernardo O'Higgins, Santiago 8370854, Chile
[3] Institute of Solid State Physics, University of Latvia, 8 Kengaraga, 1063 Riga, Latvia
* Correspondence: yanasuchikova@gmail.com

Abstract: CdxTeyOz/CdS/ZnO heterostructures were obtained by the SILAR method using ionic electrolytes. A CdS film was formed as a buffer layer for better adhesion of the cadmium-tellurium oxides to the substrate surface. In turn, the ZnO substrate was previously prepared by electrochemical etching to form a rough textured surface. In addition, an annealing mode was used in an oxygen stream to complete the oxidation process of the heterostructure surface. The resulting nanocomposite was investigated using RAMAN, XRD, SEM, and EDX methods. We assume that the oxides CdO and TeO_4 initially form on the surface and later evolve into TeO_2 and TeO_3 when saturated with oxygen. These oxides, in turn, are the components of the ternary oxides $CdTeO_3$ and $CdTe_3O_8$. It should be noted that this mechanism has not been fully studied and requires further research. However, the results presented in this article make it possible to systematize the data and experimental observations regarding the formation of cadmium-tellurium films.

Keywords: heterostructures; films; oxides; SILAR method; electrolytes; annealing

Citation: Suchikova, Y.; Kovachov, S.; Bohdanov, I.; Popova, E.; Moskina, A.; Popov, A. Characterization of $Cd_xTe_yO_z$/CdS/ZnO Heterostructures Synthesized by the SILAR Method. *Coatings* **2023**, *13*, 639. https://doi.org/10.3390/coatings13030639

Academic Editor: Panos Poulopoulos

Received: 19 February 2023
Revised: 11 March 2023
Accepted: 15 March 2023
Published: 17 March 2023

1. Introduction

The development of modern electronics and new technologies requires new materials with different properties. Significant progress in this area has been achieved by nanostructuring the surface of semiconductors which is already a well-known technique and has been studied in detail. In particular, quantum dots [1,2], nanoneedles [3,4], porous surfaces [5,6], thin films [7,8], etc., have received considerable attention. In recent years, there has been a trend toward the design of multilayer structures due to the prospect of their application in laser technology [9,10], such as optical filters [11,12], photocatalysts [13], sensors [14], and materials for solar cells [15,16].

The main technological tasks facing researchers are the search for inexpensive starting materials and simple methods of synthesis. This will make it possible to bring nanotechnology products from scientific laboratories into the industrial sector.

In this respect, semiconductors such as silicon Si [17], zinc oxide ZnO [18], cadmium sulfide CdS [19], cadmium telluride CdTe [20], etc., have received considerable attention. In particular, ZnO has been the subject of significant research for many years due to its successful synthesis technology and its promise for numerous applications [21,22]. Although ZnO has a low surface nanostructuring capacity, this material is now widely used as a substrate for the synthesis of multilayer heterostructures [23,24]. It is important to note here that, in this aspect, a wide-gap CdS semiconductor, widely used in optoelectronics and as a phosphor, can be a promising and inexpensive material [25,26]. It is more amenable to nanostructuring, which is why quantum dots [27], nanowires [28], and nanotubes [29,30] have been synthesized on its basis and studied in detail. This material is also interesting for the creation of heterostructures as visible-light-driven photocatalysts for efficient hydrogen

generation [31]. In addition, lead-free halide perovskite–COF nanocomposites are also currently being actively considered as photocatalysts [32].

CdTe films became the basis for the creation of terrestrial solar cells due to the availability of the material and its high stability. The main problem remains the search for ohmic contacts with cadmium telluride and the increase in the efficiency of cadmium-telluride solar cells [33].

In recent years, oxide semiconductors, such as Ga_2O_3 [34–36], NiO [37], and In_2O_5 [38], have gained more and more importance and interest. They exhibit quite good optoelectronic properties and high stability due to surface self-passivation [39]. Cadmium telluride oxidation technologies make it possible to obtain materials with a controlled band gap from 1.5 eV (for CdTe) to 3.8 eV, depending on the oxygen concentration [40].

It should be noted that CdTexOy materials have already been partially described and studied, particularly in the case of CdO (x = 0), CdTe (y = 0), and various tellurates: CdTeO, Cd_2TeO_4, Cd_3TeO_6, Cd_3TeO_6, $CdTe_3O_8$, $CdTe_2O_5$, and $CdTeO_3$ [41–43].

The interest in these materials is due, first of all, to the search for cheap technologies for the mass production of solar cells that do not require high-quality single crystals [44]. Additionally, the fact that the main absorption gap of CdTe is in the region of the maximum intensity of solar radiation makes it an important material for solar energy conversion [45]. Solar cells based on CdTe/CdS heterojunctions are also a valuable option [46,47]. In addition, it has been shown that O-enriched CdTe can form complex structures of $Cd_xTe_yO_z$. This highly conductive partially amorphized material can be useful in devices exposed to powerful radiation, for example, in extraterrestrial applications, where further lattice disorder caused by radiation damage would not significantly affect the performance of the device. That is, the presence of several phases in this material does not affect the efficiency of the solar cells, but, on the contrary, it positively affects its resistance to radiation [48–51]. Another article [52] emphasized that amorphous and polycrystalline $CdTeO_x$ films can be effectively used in devices that require insulating layers. Furthermore, complex $Cd_xTe_yO_z$ nanocomposites have been actively used for the manufacture of phosphors, dosimeters, and sensors [53–56].

In this work, we report the synthesis of a complex $Cd_xTe_yO_z$/CdS/ZnO multilayer heterostructure by a combination of simple methods, namely, electrochemical deposition and the SILAR method. These methods are characterized by speed, simplicity, and low cost. In addition, they allow for the controlled synthesis of structures of high quality on a large surface area. Furthermore, we investigated the chemical and structural composition of the formed heterostructure, as well as the morphological characteristics of the surface.

2. Materials and Methods

2.1. Materials and Samples for the Experiment

Preparation of the substrate. Single crystals of high-crystalline hexagonal ZnO were used as the substrate. ZnO single crystals were polished on both sides and cut into 1 cm × 1 cm × 0.5 cm plates. Before the experiment, the samples were degreased with vinegar and washed in a water-alcohol solution. To better adhere the deposited substrates to the substrate surface, texturing of the ZnO surface was carried out. For this, an anodic electrochemical reaction was carried out using electrochemical etching in a hydrochloric acid solution ($HCl:H_2O:C_2H_5OH$ = 2:1:1) at constant voltage U = 5 V for 10 min in illumination mode with a 250 W Osrm XBO xenon lamp (Osram, Regensburg, Germany) at a distance of 10 cm from the semiconductor surfaces. As a result, the microrelief containing terraces, steps, and pores was formed on the ZnO surface.

Preparation of the solution for CdS deposition (solution 1). An aqueous solution of cadmium chloride (0.1 M $CdCl_2$) was used to form a layer of cadmium sulfide (CdS). Thiourea (CH_4N_2S) and ammonia (NH_3) were added to the solution in the proportion of components:

$$CdCl_2:CH_4N_2S:NH_3 = 0.1\ M:0.1\ M:5\ M$$

The solution was heated to 80 °C with constant stirring with a magnetic stirrer for 20 min.

Solutions for the formation of $Cd_xTe_yO_z$ nanoparticles. An aqueous solution of sodium telluride (0.01 M Na_2TeO_3) was used as a tellurium source—solution 2; cadmium sources—alcoholic solution of cadmium nitrate (0.01 M $Cd(NO_3)_2$)—solution 3.

2.2. Synthesis Methods

The successive ionic layer adsorption and reaction method (SILAR) was used to synthesize the $Cd_xTe_yO_z$/CdS/ZnO heterostructure. This method includes the following necessary steps:

- Preparation of solutions containing ions of precipitated substances;
- Immersion of the substrate in the prepared solution for the purpose of adsorption of ions;
- Washing the substrate to remove excess (non-adsorbed and weakly bound) ions from its surface;
- Drying of samples.

The sample was dipped alternately into the prepared solutions. The peculiarity of the method is that between each stage of deposition (immersion in ionic solutions), it is necessary to wash the samples to remove excess reaction products. Cycles can be repeated several times to achieve the desired result. This achieves layer-by-layer adsorption which allows for the formation of multilayer heterostructures. The stages of the experiment and their durations are shown in Figure 1 and Table 1.

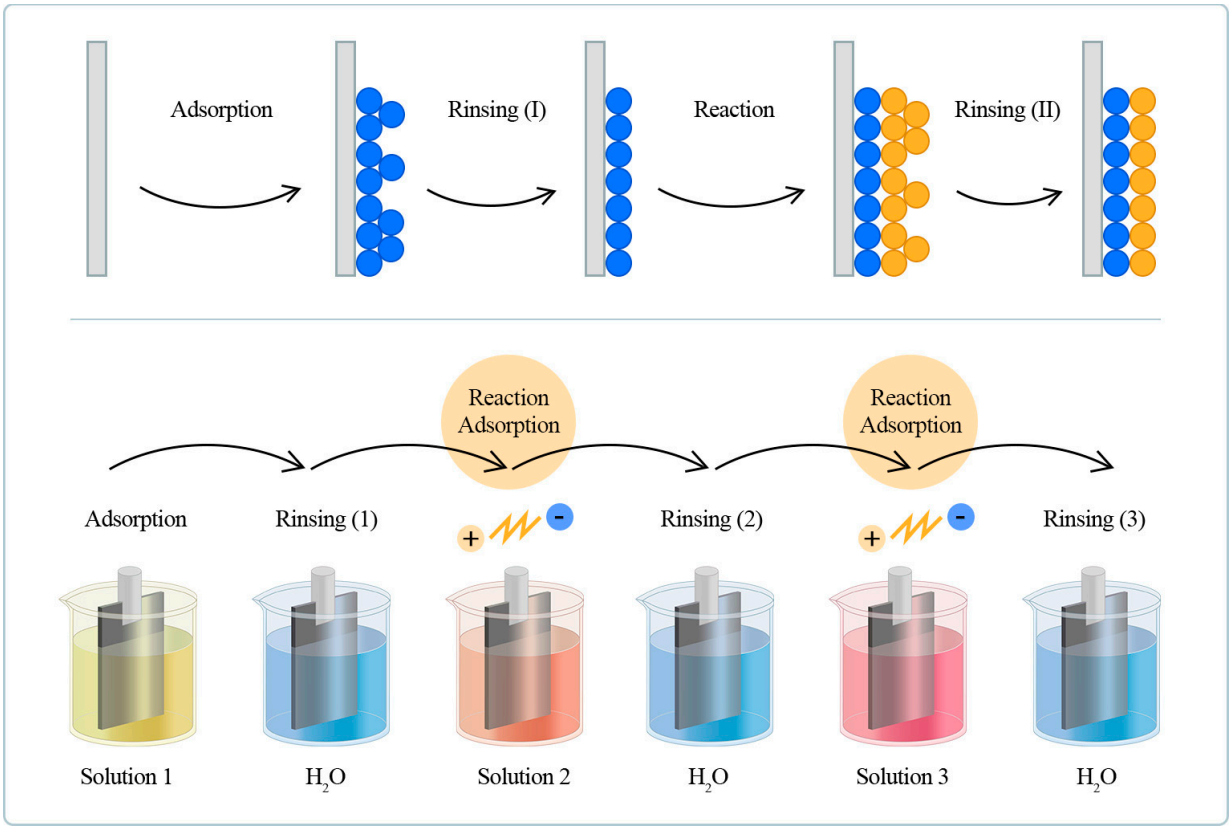

Figure 1. Scheme of the SILAR method for obtaining heterostructure $Cd_xTe_yO_z$/CdS/ZnO.

One cycle of $Cd_xTe_yO_z$ formation consisted of (3–6) stages. Five such cycles were conducted.

After the experiment, to complete the process of crystallization and oxidation, the samples were placed in the JetFirst (ECM Lab Solutions, Grenoble, France) high-speed annealing diffusion furnace in a flow of oxygen. The treatment temperature was 150 °C and the duration was 20 min.

Table 1. Stages of the layer-by-layer formation of the $Cd_xTe_yO_z$/CdS/ZnO heterostructure.

Stage №	Name, Purpose	Solution	Duration
1	Formation of CdS/ZnO structure	$CdCl_2$:CH_4N_2S:NH_3 = 0.1 M:0.1 M:5 M	5 h
2	Rinsing 1, removal of excess reaction products	Distilled H_2O	2 min
3	Formation of $Cd_xTe_yO_z$/CdS/ZnO heterostructure	Aqueous solution 0.01 M Na_2TeO_3	10 min
4	Rinsing 3, removal of excess reaction products	H_2O_2	2 min
5	Formation of CdxTeyOz/CdS/ZnO heterostructure	Alcohol solution 0.01 M $Cd(NO_3)_2$	10 min
6	Rinsing 3, removal of excess reaction products	H_2O_2	2 min

2.3. Characterization of Synthesised Structures

The morphology of the obtained structures was studied using an SEO-SEM Inspect S50-B (Novations LLC, Kyiv, Ukraine) scanning electron microscope. The chemical composition of the surface layers was studied using the EDX method on an AZtecOne spectrometer with an X-MaxN20 (Oxford Instruments Group, Oxford, UK) detector. X-ray diffraction was performed on a Dron-3 M diffractometer with unfiltered Cu Ka-radiation in the range of angles 2ϑ 10–80° with a step of 0.01°. Raman measurements were performed at room temperature in a RENISHAW inVia Reflex system (Renishaw Technology Group, Wotton-under-Edge, UK) with an excitation wavelength of 532 nm at an intensity of 5%.

To describe the morphological and structural characteristics, ImageJ (version 1.53q, 2022, Wayne Rasband and contributors, Bethesda, MD, USA), Vesta (version 3.5.7, 2021, Koichi Momma and Fujio Izumi, Tsukuba-shi, Japan), and databases of crystallographic structures Crystallography Open Database (COD) software packages and The Cambridge Crystallographic Data Centre (CCDC) software packages were used.

3. Results

3.1. SEM Analysis

Figure 2 shows an image of the surface morphology of the $Cd_xTe_yO_z$/CdS/ZnO heterostructure, taken at the maximum allowable approximation (magnification 100,000 times). As a result of the excessive magnification and translucency of the material, the quality of the image is not very high, but it allows us to assess the main morphological characteristics of the formed structure. The surface is covered with small spherical crystallites which are packed very tightly. The diameter of the crystallites is in the range of 70–90 nm (on the cutouts of the morphology image in Figure 2b). At this size of nanoobjects, the presence of quantum-dimensional effects is observed. Additionally, on the cuts of Figure 2c, one can see the presence of another phase—in these areas, the structure is denser but has pores with a cross-sectional size of 50–70 nm. Interestingly, the phases do not have clearly defined boundaries; they smoothly transition to each other, forming a loose structure. This may indicate the presence of several substances related to composition on the surface. Figure 2d shows a transverse cleavage of the resulting heterostructure. The CdS film is quite wide (2 μm), which is a consequence of the long exposure of the sample to the $CdCl_2$:CH_4N_2S:NH_3 solution, the concentration of reagents in the electrolyte [57], and the temperature of the electrolyte [58]. The $Cd_xTe_yO_z$ surface film has a much smaller width (500 nm) and exhibits a loose morphology with islands on the surface.

In addition, the interface of the heterostructure demonstrates the presence of pinholes (Figure 3). It is believed that such holes can be a consequence of the poor wettability of the substrate [59]. Such morphological defects can lead to increased surface recombination [60].

However, it was shown in [61] that the presence of narrow holes does not actually harm the performance of the device and may even improve its performance to some extent.

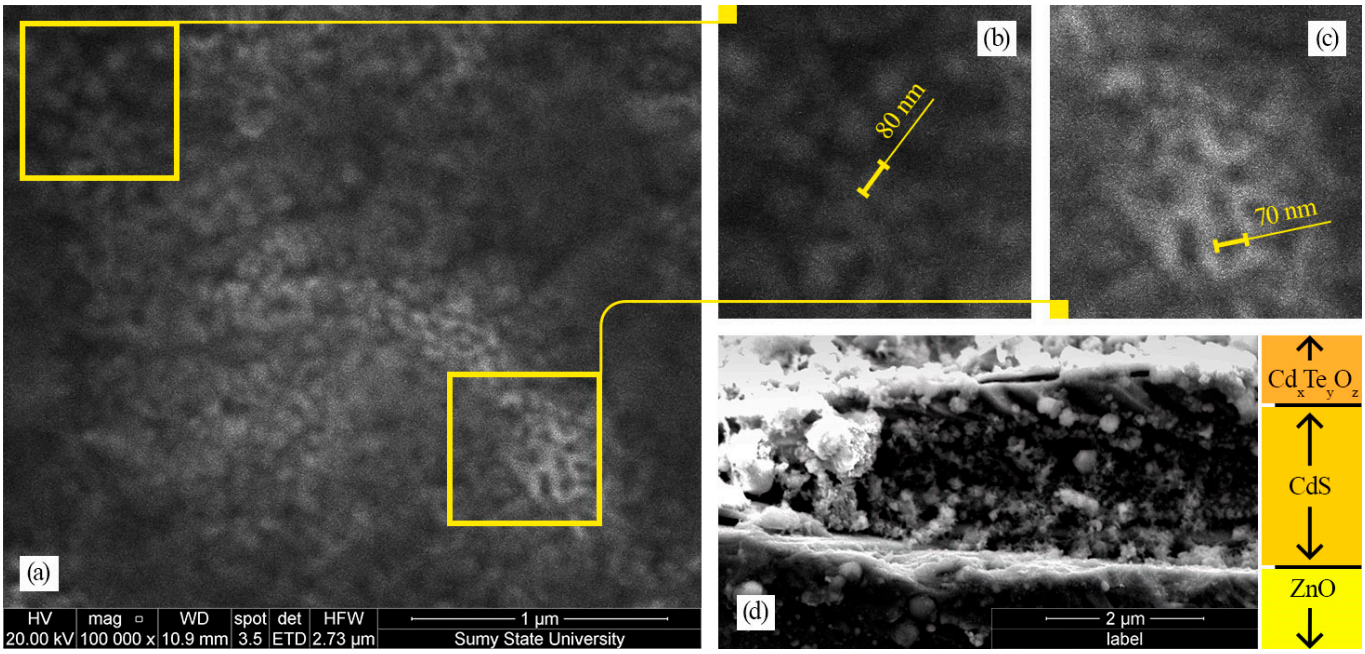

Figure 2. SEM images of the surface (**a**–**c**) and cross-sectional view (**d**) of the $Cd_xTe_yO_z$/CdS/ZnO heterostructure.

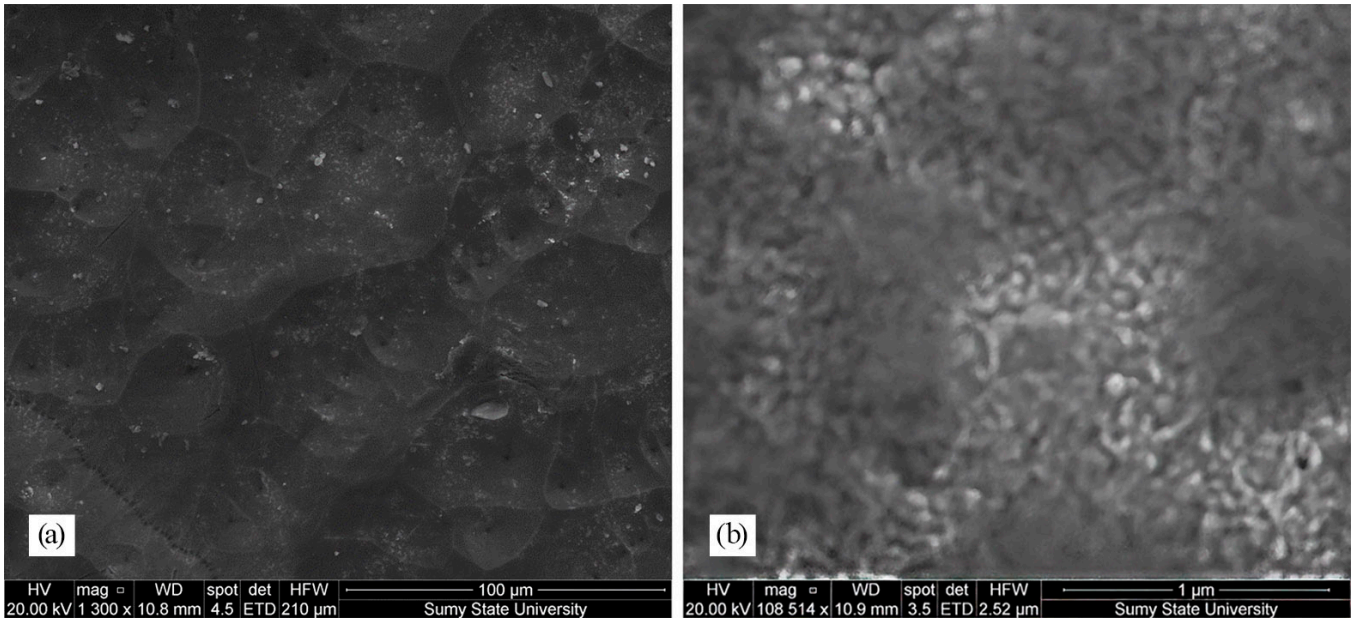

Figure 3. SEM images of the surface CdxTeyOz/CdS/ZnO heterostructure showing pinholes on the surface: (**a**) 1300× magnification shows the surface interface, (**b**) magnification of 108,514× shows the micromorphology of the surface.

3.2. EDAX Analysis

Figure 4 shows the EDX spectrum and the ratio of components on the surface of the formed structure. It can be seen that there are spectra from Zn, S, Cd, Te, and O. Zn and S are present at low concentrations (3.23% and 9.69%, respectively); this indicates that the surface of the samples is quite densely overgrown with cadmium-tellurium oxides. The

highest concentration is oxygen, which indicates its presence in various compounds of cadmium and tellurium. Reflexes of other elements were not detected.

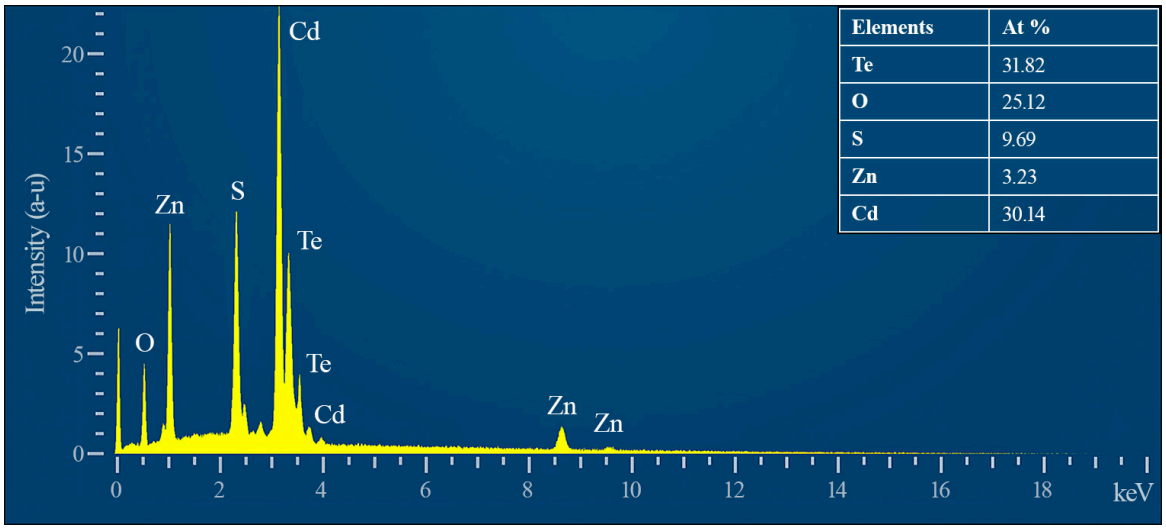

Elements	At %
Te	31.82
O	25.12
S	9.69
Zn	3.23
Cd	30.14

Figure 4. EDX spectrum and component composition of the CdxTeyOz/CdS/ZnO surface.

3.3. XRD Analysis

Figure 5 shows the diffractometric spectra of the formed structure. The main peak corresponds to the (310) plane of $CdTe_3O_8$ (Monoclinic, Space group P2/c, Space group number 13; a = 14.0660 A; b = 5.8720 A; and c = 10.5210 A). The crystallite size calculated by Scherrer's formula from this spectrum is 24.9 nm. Additionally, the diffraction peaks at 2θ = 20.82, 27.805, 28.513, and 33.74 correspond to the (111), (112), (440), and (020) planes of the monoclinic structure $CdTe_3O_8$, respectively. Peaks associated with $CdTeO_3$ are observed at 2θ = 31.4, 54.40, 63.85, and 75.75, which correspond to the (040), (220), (004), and (110) planes of the orthomorphic structure, respectively. The intensity of these peaks is very weak compared to the peaks associated with $CdTe_3O_8$. This indicates the predominance of $CdTe_3O_8$ oxide over $CdTeO_3$ on the surface of the synthesized structure.

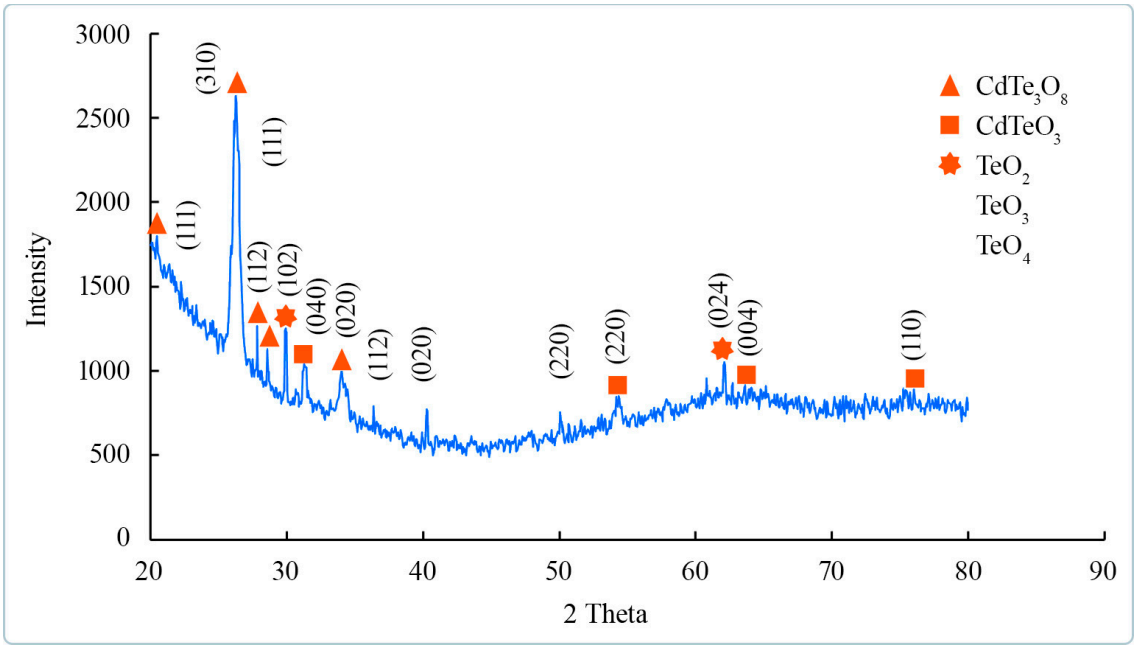

Figure 5. XRD spectrum of the $Cd_xTe_yO_z$/CdS/ZnO heterostructure.

No CdS peaks were detected. This may indicate a fairly dense $Cd_xTe_yO_z$ nanocomposite film embedded in the matrix of the substrate. It may also indicate that the surface of the CdS/ZnO heterostructure was characterized by the presence of an oxide amorphized layer.

In addition, it is possible to determine the presence of peaks from tellurium oxides TeO_2, TeO_3, and TeO_4. Their weak intensity and proximity to the peaks of $CdTe_3O_8$ and $CdTeO_3$ indicate that tellurium oxides are components of the structures of cadmium-tellurium oxides. When $CdTe_3O_8$ is oversaturated with oxygen over $CdTeO_3$, it can replace it with cadmium and form the compound TeO_3 [62]. The transition to TeO_4 also occurs due to the addition of oxygen:

$$TeO_3 + O_2 \rightarrow TeO_4$$

Noise is present in the right region of the spectrum, a halo is present in the (50–70) 2θ region, and a very weak intensity indicates surface amorphization due to the transition from $CdTe_3O_8$ and $CdTeO_3$ oxides to TeO_4 and TeO_2. Furthermore, in [63], the haloes are associated with the presence of TeO_2. Evidence of the presence of tellurium oxides is also seen in the yellow color of the sample surface, which is characteristic of the amorphous α-TeO_3 phase. These results agree well with the previously made assumption of the presence of several oxides on the surface of the synthesized heterostructure.

3.4. Raman Analysis

The Raman spectrum demonstrates the presence of spectra of high (300 cm^{-1}, 603 cm^{-1}) and medium (108 cm^{-1}, 211 cm^{-1}, 253 cm^{-1}) intensity (Figure 6). Some peaks extend from the right edge and have minor low-intensity peaks (e.g., 145 cm^{-1}, 319 cm^{-1}, and 369 cm^{-1}). It can also be seen that starting from 600 cm^{-1} and above, there is a sharp rise in the spectrum line ("tail").

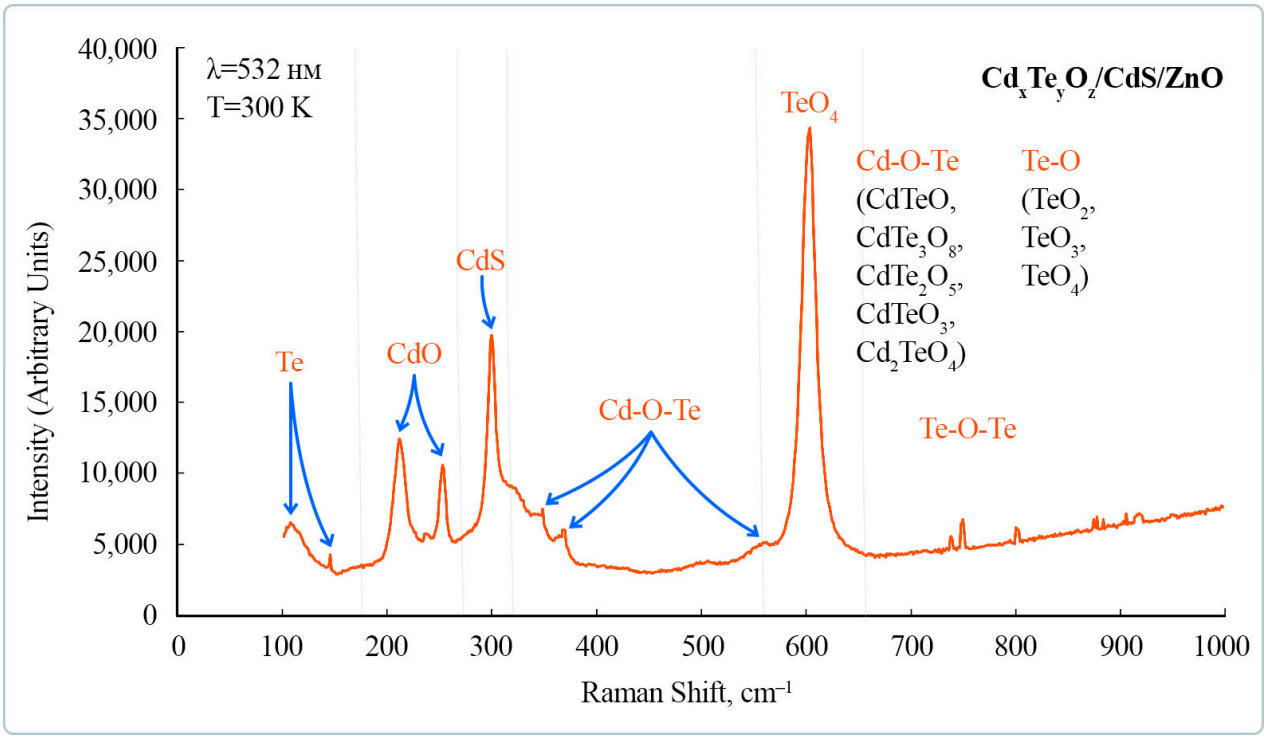

Figure 6. Raman scattering spectra of the $Cd_xTe_yO_z$/CdS/ZnO heterostructure.

Spectra from the ZnO substrate were not recorded. This indicates the complete overgrowth of the surface with cadmium-containing films of sufficient thickness. The intense peak at 300 cm^{-1} is due to the main LO phonon mode of CdS. This peak is asymmetric toward a higher frequency compared to the typical spectrum of bulk CdS

(305 cm^{-1}). It also contains minor peaks at 248 and 369 $cm^{-1.}$ which may indicate the presence of particles with a large spread in size.

The low-frequency peaks at 108 cm^{-1} and 145 cm^{-1} are attributed to zone-centered phonons of crystalline Te (A1 and E-symmetry, respectively). The intensity of the peak at 108 cm^{-1} is medium, while that of the peak at 145 cm^{-1} is quite weak. This indicates a low concentration of free crystalline tellurium on the surface of the formed structure.

The peak at 253 cm^{-1} is typical for the cubic phase of cadmium oxide (CdO). A peak in the region of 211 cm^{-1} is also attributed to CdO. Its shift to the low-frequency region of the spectrum compared to the typical one (216 cm^{-1}) and a rather large width indicate the presence of nanometer-sized particles.

It is interesting to note that typical CdTe peaks (165 cm^{-1} and 325 cm^{-1}) [64] are not observed. However, there is strong noise in the 310–370 cm^{-1} region, because of which there is a rightward broadening of the 300 cm^{-1} peak. The appearance of such noise indicates that the surface of the structure was completely oxidized with the formation of various oxide compounds of Cd and Te.

That is, during the ion deposition and annealing of samples in an oxygen stream, we formed the compound $Cd_xTe_yO_z$. Extreme cases are those when one of the coefficients becomes zero (Te_yO_z, Cd_xTe_y, and Cd_xO_z at x = 0, y = 0, and z = 0, respectively).

The most intense peak at 603 cm^{-1} can be associated with the first overtone mode of 2LO CdS. However, there are reports that indicate that the intense peaks in the region of 550–600 cm^{-1} are due to the vibrational modes of TeO_4 [65]. At the same time, the intensity of the spectrum depends on the concentration of oxygen in the compounds. That is, the TeO_4 compound is present in various types of cadmium-tellurium oxide. Note that in our case, the intensity of the peak may be caused by the manifestation of quantum-size effects owing to the presence of nanometer-sized crystallites. This size of the crystallites allows them to be classified as quantum dots.

In the 600 to 800 cm^{-1} region, low-intensity vibrational modes are observed which are related to the Te-O-Te vibrational bonds. It can be argued that TeO_3, when saturated with oxygen, changes to the form TeO_4, which is observed in oxides $CdTeO_3$ and $CdTe_3O_8$. In the Raman light scattering spectrum, peaks from these structural units are observed in the region of 850–950 cm^{-1}. The intensity of the spectra in the region after 603 cm^{-1} is very low and has a rather fluctuating characteristic. This indicates a significant amorphization of the structure and the formation of glassy oxides, which are tellurium oxides ($TeO_2 \rightarrow TeO_3 \rightarrow TeO_4$). This is also evidenced by the formation of a "tail" of the spectrum in the high-frequency region. These results agree well with the XRD and SEM analysis results.

In other words, at low oxygen concentrations, TeO_4 compounds are formed which are compatible with orthorhombic oxide $CdTeO_3$ [66]. When the structures are oversaturated with oxygen, oxygen atoms displace cadmium atoms with the formation of the TeO_3 compound. Then, it becomes possible to transition to TeO_2 oxide, which can be a component of $CdTe_3O_8$, $CdTe_2O_5$, and CdTeO compounds [67].

4. Discussion

The SILAR method is based on the adsorption of ionic particles of solutions on the substrate surface. Adsorption triggers a chemical reaction at the interface which leads to the formation of an insoluble product. This is why the primary precursor from which the thin film is formed is of crucial importance (Table 1). The atoms of this film will be adsorption centers for the further deposition of material. The removal of excess and weakly bonded atoms is a crucial factor for the good adhesion of films to the substrate. Therefore, washing the sample is an important step (Figure 1).

The method of heterostructure growth chosen by us is characterized by a gradual transition from one phase to another which allows for the removal of elastic deformations at the interface of two materials. Thus, the porous layer formed on the ZnO surface acts as a buffer layer for the CdS film which crystallizes in a hexagonal lattice similar to that of ZnO but differs in the crystal lattice parameters. This buffer layer helps minimize the effects

of lattice mismatch. Then, by oxidation of the CdS surface, cubic CdO is formed. When processing this structure in electrolytes containing tellurium, a complex nanocomposite containing TeO_2, TeO_3, TeO_4, $CdTeO_3$, and $CdTe_3O_8$ is formed. The composition and thickness of the film depend significantly on the exposure time in the precursors.

This method is a modification of the chemical precipitation method, and its advantages include simplicity, cost effectiveness, the ability to quickly generate large-area films, and the capability of controlling the composition of the film over a wide range without requiring a vacuum or special temperatures [67,68].

However, the adhesion of the material to the substrate may be insufficient because of the weak interaction and incoherence of the crystal lattices. Therefore, it is advisable to use a buffer layer. The CdS buffer layer we used allowed us to effectively form a film of cadmium tellurium oxide. In [69], a layer of cadmium sulfide was also used to grow CuS films. The authors showed that such a buffer significantly improves the adhesion of the film to the substrate. Therefore, compared to ZnO, CdS shows a better affinity for crystal lattices with the synthesized materials CdO, $CdTeO_3$, and $CdTe_3O_8$ (Table 2, Figure 7). Thus, CdS serves as a reliable buffer layer and, thanks to oxidation, allows for the formation of a transition layer of CdO for the further formation of $Cd_xTe_yO_z$.

Table 2. Crystal lattice parameters of ZnO, CdS, CdTe, CdO, TeO_2, TeO_3, TeO_4, $CdTeO_3$, and $CdTe_3O_8$.

Characteristic	ZnO	CdS	CdTe	CdO	TeO_2	TeO_3	TeO_4	$CdTeO_3$	$CdTe_3O_8$
COD number	1,011,258	1,011,054	-	1,011,003	9,008,125	7,035,629	-	7,041,644	-
Crystal system	Hexagonal	Hexagonal	Hexagonal	Cubic	Orthorhombic	Trigonal	Monoclinic	Orthorhombic	Monoclinic
Space group	P63-mc	P63mc	P63mc	Fm-3 m	Pbca	R-3c	P2/c	Pnma	P2/c
Space group number	186	186	186	225	61	167	14	62	13
Volume of cell, $Å^{-3}$	46.692	104.86	145.82	103.76	395.35	97.26	136.77	1196.38	771.50
a, Å	3.220	4.207	4.684	4.699	5.6	5.285	4.96	7.458	14.066
b, Å	3.220	4.207	4.684	4.699	5.75	5.285	5.23	14.522	5.872
c, Å	5.220	6.843	7.674	4.699	12.3	5.285	5.77	11.046	10.521
α, °	90	90	90	90	90	57.051	65.83	90	90
β, °	90	90	90	90	90	57.051	90	90	117.4
γ, °	120	120	120	90	90	57.051	90	90	90

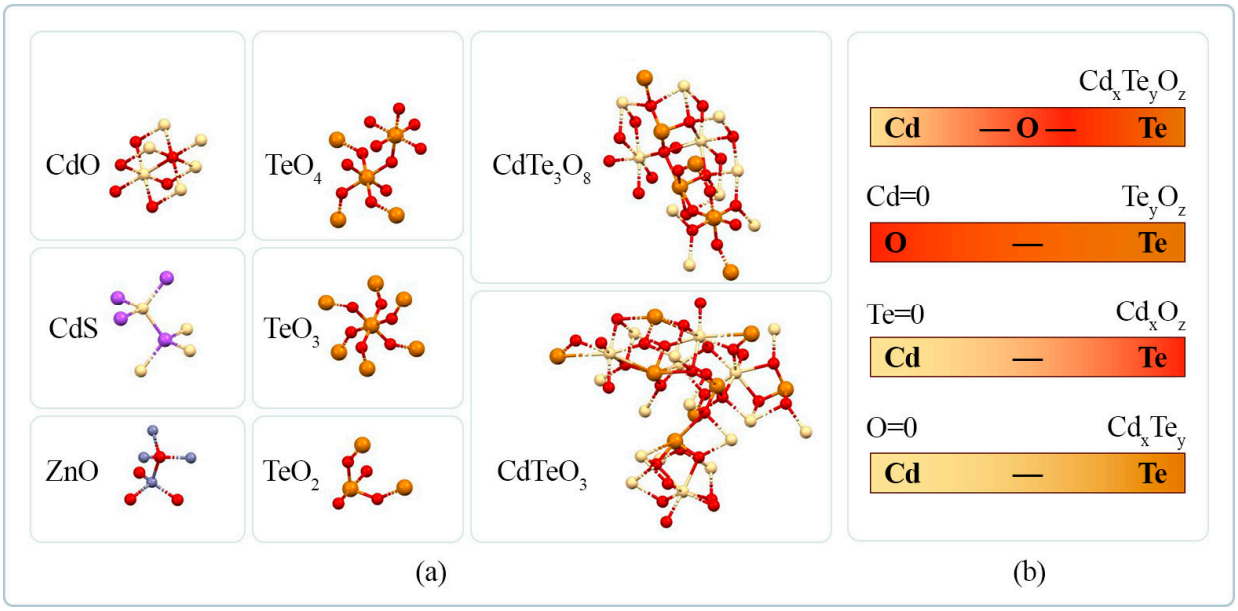

Figure 7. Crystal lattices of the materials that make up the $Cd_xTe_yO_z$/CdS/ZnO heterostructure (**a**) and a schematic representation of probable $Cd_xTe_yO_z$ oxides at different concentrations of elements (**b**).

Solid CdTe crystallizes in a hexagonal crystal lattice of the sphalerite type [70], and the cadmium and tellurium atoms each have four paired atoms of a different type which are located in the vertices of the tetrahedron. Instead, CdO crystallizes in a cubic rock salt-like crystal lattice. The Cd and O atoms each have six bonds with atoms of different types (Table 2). For these reasons, CdTe and CdS exhibit a crystal lattice match compared to the CdS and CdO pair. The absence of Raman peaks from CdTe indicates that Cd–O and Te–O bonds are formed by oxygen absorption, which may block the formation of Cd–Te bonds [71]. In addition, the formation of CdTe on the surface of CdS is energetically disadvantageous compared to CdO because of the higher chemical activity of oxygen ions in the electrolyte, which may be represented by the hydroxyl group.

The results of the experimental data indicate that the formed heterostructure contains a dense layer of $Cd_xTe_yO_z$/CdS/ZnO oxide. Therefore, the binary oxides TeO_2 and TeO_4 are detected on the surface.

Table 2 also shows the affinity of the binary oxides TeO_2 and TeO_4 with the ternary compounds $CdTeO_3$ and $CdTe_3O_8$, respectively. Figure 6 shows that TeO_2 is bonded to four oxygen atoms, while TeO_4 and TeO_3 have six bonds each, with the difference that TeO_4 has one non-bridging oxygen, that is, it is bonded to only one oxygen atom. The ternary crystals of $CdTeO_3$ and $CdTe_3O_8$ have only Cd-O and Te-O bonds, but no Cd-Te bonds [72]. On this basis, it can be assumed that the oxides CdO and TeO_4 initially form on the surface and later evolve into TeO_2 and TeO_3 when saturated with oxygen. These oxides, in turn, are components of the ternary oxides $CdTeO_3$ and $CdTe_3O_8$.

The resulting nanocomposite may be interesting for applications in optical waveguides, photonic devices, and solar cells because of the ability to adjust the optical energy gap by controlling the oxygen content in the oxide lamonas. Further research should aim to establish and optimize all stages of the technological process for the synthesis of $Cd_xTe_yO_z$/CdS/ZnO heterostructures with a predetermined composition of components.

5. Conclusions

We have demonstrated the possibility of forming a $Cd_xTe_yO_z$/CdS/ZnO heterostructure using a simple and inexpensive SILAR method. For this purpose, a six-step procedure was applied, three of which involved keeping the sample in ionic electrolytes, and another three which involved washing the samples in distilled water to remove weakly bound atoms from the surface. This, in turn, ensured good adhesion of the films.

Morphological analysis of the obtained heterostructure showed the presence of nanometer-sized spherical islands. According to the results of X-ray structural analysis and Raman light scattering, binary and ternary oxides $Cd_xTe_yO_z$ are formed on the surface of the heterostructure, which are in both crystalline and amorphous phases. The presence of CdTe on the surface of the structure was not recorded.

Author Contributions: Conceptualization, Y.S. and A.P.; Methodology, Y.S. and S.K.; Software, S.K.; Validation, S.K.; Formal analysis, A.M.; Investigation, Y.S. and E.P.; Resources, Y.S., I.B. and A.P.; Writing—original draft, Y.S. and I.B.; Writing—review and editing, A.P.; Funding acquisition, A.P. All authors have read and agreed to the published version of the manuscript.

Funding: The study was supported by the Ministry of Education and Science of Ukraine via Project No. 0122U000129 "The search for optimal conditions for nanostructure synthesis on the surface of A3B5, A2B6 semiconductors and silicon for photonics and solar energy" and Project No. 0121U10942 "Theoretical and methodological bases of system fundamentalization of the future nanomaterials experts training for productive professional activity". In addition, the research of A.P. and Y.S. was partly supported by COST Action CA20129 "Multiscale Irradiation and Chemistry Driven Processes and Related Technologies" (MultIChem). A.P. thanks to the Institute of Solid-State Physics, University of Latvia. ISSP UL as the Center of Excellence is supported through the Framework Program for European universities, Union Horizon 2020, H2020-WIDESPREAD-01–2016–2017-TeamingPhase2, under Grant Agreement No. 739508, CAMART2 project.

Institutional Review Board Statement: Not applicable.

Informed Consent Statement: Not applicable.

Data Availability Statement: Data sharing is not applicable to this article.

Conflicts of Interest: The authors declare no conflict of interest.

References

1. García de Arquer, F.P.; Talapin, D.V.; Klimov, V.I.; Arakawa, Y.; Bayer, M.; Sargent, E.H. Semiconductor quantum dots: Technological progress and future challenges. *Science* **2021**, *373*, 8541. [CrossRef] [PubMed]
2. Li, M.; Chen, T.; Gooding, J.J.; Liu, J. Review of carbon and graphene quantum dots for sensing. *ACS Sens.* **2019**, *4*, 1732–1748. [CrossRef]
3. Karbovnyk, I.; Savchyn, P.; Huczko, A.; Mirr, C.; Popov, A.I. FTIR studies of silicon carbide 1D- nanostructures. *Mater. Sci. Forum* **2015**, *821–823*, 261–264. [CrossRef]
4. Suohikova, Y.; Vambol, S.; Vambol, V.; Mozaffari, N.; Mozaffari, N. Justification of the most rational method for the nanostructures synthesis on the semiconductors surface. *J. Achiev. Mater. Manuf. Eng.* **2019**, *92*, 19–28.
5. Suchikova, Y. Provision of environmental safety through the use of porous semiconductors for solar energy sector. *East.-Eur. J. Enterp. Technol.* **2016**, *6*, 26–33. [CrossRef]
6. Yana, S. Porous indium phosphide: Preparation and properties. In *Handbook of Nanoelectrochemistry: Electrochemical Synthesis Methods, Properties, and Characterization Techniques*; Springer: Berlin/Heidelberg, Germany, 2016; pp. 283–306.
7. Abadias, G.; Chason, E.; Keckes, J.; Sebastiani, M.; Thompson, G.B. Stress in thin films and coatings: Current status, challenges, and prospects. *J. Vac. Sci. Technol. A Vac. Surf. Films* **2018**, *36*, 020801. [CrossRef]
8. Chen, S.; Yuan, S.; Hou, Z.; Tang, Y.; Zhang, J.; Chen, Z. Recent progress on topological structures in ferroic thin films and heterostructures. *Adv. Mater.* **2021**, *33*, 2000857. [CrossRef]
9. Suchikova, J.A.; Kidalov, V.V.; Sukach, G.A. Blueshift of photoluminescence spectrum of porous InP. *ECS Trans.* **2009**, *25*, 59–64. [CrossRef]
10. Huczko, A.; Dabrowska, A.; Savchyn, V.; Popov, A.I.; Karbovnyk, I. Silicon carbide nanowires: Synthesis and cathodoluminescence. *Phys. Status Solidi (B) Basic Res.* **2009**, *246*, 2806–2808. [CrossRef]
11. Pan, H.Y.; Chen, X.; Xia, X.L. A review on the evolvement of optical-frequency filtering in photonic devices in 2016–2021. *Renew. Sustain. Energy Rev.* **2022**, *161*, 112361. [CrossRef]
12. Kawanishi, T. Precise optical modulation and its application to optoelectronic device measurement. *Photonics* **2021**, *8*, 160. [CrossRef]
13. Yang, Q.; Dong, L.; Su, R.; Hu, B.; Wang, Z.; Dong, M. Nanostructured heterogeneous photocatalysts for hydrogen production and water splitting: A comprehensive insight. *Appl. Mater. Today* **2019**, *17*, 159–182. [CrossRef]
14. Suchikova, Y.A.; Kidalov, V.V.; Sukach, G.A. Influence of the carrier concentration of indium phosphide on the porous layer formation. *J. Nano- Electron. Phys.* **2010**, *2*, 75–81.
15. Vambol, S.; Vambol, V.; Suchikova, Y.; Deyneko, N. Analysis of the ways to provide ecological safety for the products of nanotechnologies throughout their life cycle. *East. -Eur. J. Enterp. Technol.* **2017**, *1*, 27–36. [CrossRef]
16. Suchikova, Y.; Bohdanov, I.; Kovachov, S.; Popov, A.I. Texturing of indium phosphide for improving the characteristics of space solar cells. In Proceedings of the IEEE 12th International Conference on Electronics and Information Technologies, ELIT 2021—Proceedings, Lviv, Ukraine, 19–21 May 2021; pp. 194–197.
17. Vambol, S.; Bogdanov, I.; Vambol, V.; Hurenko, O.; Onishchenko, S. Research into regularities of pore formation on the surface of semiconductors. *East. -Eur. J. Enterp. Technol.* **2017**, *3*, 37–44. [CrossRef]
18. Goktas, S.; Goktas, A. A comparative study on recent progress in efficient ZnO based nanocomposite and heterojunction photocatalysts: A review. *J. Alloy. Compd.* **2021**, *863*, 158734. [CrossRef]
19. Cheng, L.; Xiang, Q.; Liao, Y.; Zhang, H. CdS-based photocatalysts. *Energy Environ. Sci.* **2018**, *11*, 1362–1391. [CrossRef]
20. Romeo, A.; Artegiani, E. CdTe-based thin film solar cells: Past, present and future. *Energies* **2021**, *14*, 1684. [CrossRef]
21. Usseinov, A.B.; Akilbekov, A.T.; Kotomin, E.A.; Karipbayev, Z.T. The first principles calculations of CO_2 adsorption on (1010) ZnO surface. *AIP Conf. Proc.* **2019**, *2174*, 020181.
22. Uklein, A.V.; Multian, V.V.; Kuz'micheva, G.M.; Gayvoronsky, V.Y. Nonlinear optical response of bulk ZnO crystals with different content of intrinsic defects. *Opt. Mater.* **2018**, *84*, 738–747. [CrossRef]
23. Suchikova, Y.; Lazarenko, A.; Kovachov, S.; Bardus, I.; Bohdanov, I. Formation of CdO/CdS/textured-ZnO/ZnO heterostructures by chemical deposition. *Phys. Chem. Solid State* **2022**, *23*, 361–367. [CrossRef]
24. Zhilova, O.V.; Pankov, S.; Sitnikov, A.V.; Makagonov, V.A. Optical and electrical properties of thin-film heterostructures of the In_2O_3–ZnO system. *Mater. Res. Express* **2019**, *6*, 086330. [CrossRef]
25. Chen, Y.; Xing, W.; Liu, Y.; Zhang, X.; Xu, S. Efficient and stable CdSe/CdS/ZnS quantum rods-in-matrix assembly for white LED application. *Nanomaterials* **2020**, *10*, 317. [CrossRef] [PubMed]
26. Zhang, G.; Bai, Y.; Yu, C.; Xuan, T. Highly stable carbon nanodot-based phosphor as a color converter for WLED. *J. Lumin.* **2022**, *246*, 118836. [CrossRef]

27. Wang, F.; Hou, T.; Zhao, X.; Li, Y. Ordered macroporous carbonous frameworks implanted with CdS quantum dots for efficient photocatalytic CO_2 reduction. *Adv. Mater.* **2021**, *33*, 2102690. [CrossRef] [PubMed]
28. Lu, K.Q.; Qi, M.Y.; Tang, Z.R.; Xu, Y.J. Earth-abundant MoS_2 and cobalt phosphate dual cocatalysts on 1D CdS nanowires for boosting photocatalytic hydrogen production. *Langmuir* **2019**, *35*, 11056–11065. [CrossRef]
29. Lu, H.; Liu, Y.; Zhang, S.; Wan, J.; Wang, X.; Deng, L.; Kan, J.; Wu, G. Clustered tubular S-scheme ZnO/CdS heterojunctions for enhanced photocatalytic hydrogen production. *Mater. Sci. Eng. B* **2023**, *289*, 116282. [CrossRef]
30. Wang, R.; Chen, S.; Ng, Y.H.; Gao, Q.; Zhang, S. ZnO/CdS/PbS nanotube arrays with multiheterojunctions for efficient visible-light-driven photoelectrochemical hydrogen evolution. *Chem. Eng. J.* **2019**, *362*, 658–666. [CrossRef]
31. Yin, X.L.; Liu, J.; Jiang, W.J.; Zhang, X.; Hu, J.S.; Wan, L.J. Urchin-like Au@ CdS/WO 3 micro/nano heterostructure as a visible-light driven photocatalyst for efficient hydrogen generation. *Chem. Commun.* **2015**, *51*, 13842–13845. [CrossRef]
32. Zhu, Y.; Liu, Y.; Ai, Q.; Gao, G.; Yuan, L.; Fang, Q.; Tian, X.; Zhang, X.; Egap, E.; Ajayan, P.M.; et al. In situ synthesis of lead-free halide perovskite–COF nanocomposites as photocatalysts for photoinduced polymerization in both organic and aqueous phases. *ACS Mater. Lett.* **2022**, *4*, 464–471. [CrossRef]
33. Khrypunov, G.; Vambol, S.; Deyneko, N.; Suchikova, Y. Increasing the efficiency of film solar cells based on cadmium telluride. *East. -Eur. J. Enterp. Technol.* **2016**, *6*, 12–18. [CrossRef]
34. Usseinov, A.; Koishybayeva, Z.; Platonenko, A.; Popov, A.I. Vacancy defects in Ga_2O_3: First-principles calculations of electronic structure. *Materials* **2021**, *14*, 7384. [CrossRef] [PubMed]
35. Usseinov, A.; Koishybayeva, Z.; Platonenko, A.; Popov, A.I. Ab-Initio Calculations of Oxygen Vacancy in Ga2O3Crystals. *Latv. J. Phys. Tech. Sci.* **2021**, *58*, 3–10.
36. Luchechko, A.; Vasyltsiv, V.; Kostyk, L.; Tsvetkova, O.; Popov, A.I. Shallow and deep trap levels in X-ray irradiated β-Ga2O3: Mg. *Nucl. Instrum. Methods Phys. Res. Sect. B: Beam Interact. Mater. At.* **2019**, *441*, 12–17. [CrossRef]
37. Suchikova, Y.; Bohdanov, I.; Kovachov, S.; Popov, A.I. The Synthesis of porous indium phosphide with nickel oxide crystallites on the surface. *J. Electrochem. Sci. Eng.* **2022**, *12*, 593–601. [CrossRef]
38. Suchikova, Y.O.; Bogdanov, I.T.; Kovachov, S.S. Oxide crystals on the surface of porous indium phosphide. *Arch. Mater. Sci. Eng.* **2019**, *98*, 49–56. [CrossRef]
39. Suchikova, Y.; Lazarenko, A.; Kovachov, S.; Popov, A.I. Formation of porous Ga_2O_3/GaAs layers for electronic devices. In Proceedings of the 16th International Conference on Advanced Trends in Radioelectronics, Telecommunications and Computer Engineering, TCSET, Lviv-Slavske, Ukraine, 22–26 February 2022; pp. 410–413.
40. Muftah, G.E.A.; Hassan, M.; Dharmadasa, I.M. Electrodeposited CdTe Thin Film Solar Cells: Chloride Treatment and Improved Efficiency. *Int. J. Eng. Innov. Res.* **2018**, *7*, 2277–5668.
41. Balakhayeva, R.; Akilbekov, A.; Baimukhanov, Z.; Popov, A.I.; Dauletbekova, A. CdTe Nanocrystal Synthesis in SiO_2/Si Ion-Track Template: The Study of Electronic and Structural Properties. *Phys. Status Solidi (A) Appl. Mater. Sci.* **2021**, *218*, 2000231. [CrossRef]
42. Akilbekov, A.; Balakhayeva, R.; Zdorovets, M.; Popov, A.I.; Dauletbekova, A. Ion track template technology for fabrication of CdTe and CdO nanocrystals. *Nucl. Instrum. Methods Phys. Res. Sect. B: Beam Interact. Mater. At.* **2020**, *481*, 30–34. [CrossRef]
43. Krämer, V.; Brandt, G. Structure of cadmium tellurate (IV), $CdTeO_3$. *Acta Crystallogr. Sect. C: Cryst. Struct. Commun.* **1985**, *41*, 1152–1154. [CrossRef]
44. Menéndez-Proupin, E.; Gutiérrez, G.; Palmero, E.; Peña, J.L. Electronic structure of crystalline binary and ternary Cd− Te− O compounds. *Phys. Rev. B* **2004**, *70*, 035112. [CrossRef]
45. Heiba, Z.K. X-ray structural phase analysis of CdTe semiconductor annealed in air. *Cryst. Res. Technol. J. Exp. Ind. Crystallogr.* **2003**, *38*, 488–493. [CrossRef]
46. Durose, K.; Boyle, D.; Abken, A.; Ottley, C.J.; Nollet, P.; Degrave, S.; Bonnet, D. Key aspects of CdTe/CdS solar cells. *Phys. Status Solidi (B)* **2002**, *229*, 1055–1064. [CrossRef]
47. Jiménez-Sandoval, S.; Garnett-Ruiz, G.E.; Santos-Cruz, J.; Jiménez-Sandoval, O.; Torres-Delgado, G.; Castanedo-Pérez, R.; Morales-Sanchez, E. Band gap tuning and high electrical conductivity in amorphous and polycrystalline films of the $Cu_x(CdTe)_yO_z$ system. *J. Appl. Phys.* **2006**, *100*, 113713. [CrossRef]
48. Ramírez-Bon, R.; Espinoza-Beltrán, F.J.; Arizpe-Chávez, H.; Zelaya-Angel, O.; Sánchez-Sinencio, F. Structural and optical studies in a-CdTe: O annealed films. *J. Appl. Phys.* **1996**, *79*, 7682–7687. [CrossRef]
49. El Azhari, M.Y.; Azizan, M.; Bennouna, A.; Outzourhit, A.; Ameziane, E.L.; Brunel, M. Optical properties of oxygenated amorphous cadmium telluride thin films. *Sol. Energy Mater. Sol. Cells* **1997**, *45*, 341–352. [CrossRef]
50. Bartolo-Pérez, P.; Castro-Rodrıguez, R.; Caballero-Briones, F.; Cauich, W.; Peña, J.L.; Farias, M.H. X-Ray photoelectron spectroscopy study of CdTe oxide films grown by rf sputtering with an Ar–NH3 plasma. *Surf. Coat. Technol.* **2002**, *155*, 16–20. [CrossRef]
51. Hussain, O.M.; Reddy, P.J. Characterization of thin film n-CdS/p-CdTe heterojunctions. *Vacuum* **1991**, *42*, 657–659. [CrossRef]
52. El Azhari, M.Y.; Azizan, M.; Bennouna, A.; Outzourhit, A.; Ameziane, E.L.; Brunel, M. Preparation and characterization of $CdTeO_3$ thin films. *Thin Solid Films* **2000**, *366*, 82–87. [CrossRef]
53. Kovachov, S.; Bohdanov, I.; Karipbayev, Z.; Suchikova, Y.; Tsebriienko, T.; Popov, A.I. Layer-by-Layer Synthesis and Analysis of the the Phase Composition of $Cd_xTe_yO_z$/CdS/por-ZnO/ZnO Heterostructure. In Proceedings of the IEEE 3rd KhPI Week on Advanced Technology (KhPIWeek), Kharkiv, Ukraine, 3–7 October 2022; pp. 1–6.

54. Guillén-Cervantes, A.; Becerril-Silva, M.; Silva-López, H.E.; Arias-Cerón, J.S.; Campos-González, E.; Pérez-González, M.; Zelaya-Ángel, O. Structural and optical properties of CdTe+ CdTeO 3 nanocomposite films with broad blueish photoluminescence. *J. Mater. Sci. Mater. Electron.* **2020**, *31*, 7133–7140. [CrossRef]
55. Oh, K.; Han, M.; Kim, K.; Heo, Y.; Moon, C.; Park, S.; Nam, S. Development and evaluation of polycrystalline cadmium telluride dosimeters for accurate quality assurance in radiation therapy. *J. Instrum.* **2016**, *11*, C02040. [CrossRef]
56. Hussin, R.; Leong, N.S.; Alias, N.S. Structural investigation of crystalline host phosphor cadmium tellurite systems. *Malays. J. Fundam. Appl. Sci.* **2009**, *5*, 17–27. [CrossRef]
57. Devi, R.A.; Latha, M.; Velumani, S.; Oza, G.; Reyes-Figueroa, P.; Rohini, M.; Becerril-Juarez, I.G.; Lee, J.-H.; Yi, J. Synthesis and characterization of cadmium sulfide nanoparticles by chemical precipitation method. *J. Nanosci. Nanotechnol.* **2015**, *15*, 8434–8439. [CrossRef] [PubMed]
58. Najm, A.S.; Naeem, H.S.; Alwarid, D.A.R.M.; Aljuhani, A.; Hasbullah, S.A.; Hasan, H.A.; Sopian, K.; Bais, B.; Al-Iessa, H.J.; Majdi, H.S.; et al. Mechanism of Chemical Bath Deposition of CdS Thin Films: Influence of Sulphur Precursor Concentration on Microstructural and Optoelectronic Characterizations. *Coatings* **2022**, *12*, 1400. [CrossRef]
59. Wu, Y.; Yang, X.; Chen, H.; Zhang, K.; Qin, C.; Liu, J.; Peng, W.; Islam, A.; Bi, E.; Ye, F.; et al. Highly compact TiO2 layer for efficient hole-blocking in perovskite solar cells. *Appl. Phys. Express* **2014**, *7*, 052301. [CrossRef]
60. Yang, G.; Tao, H.; Qin, P.; Ke, W.; Fang, G. Recent progress in electron selective layers for efficient perovskite solar cells. *J. Mater. Chem. A* **2016**, *4*, 3970–3990. [CrossRef]
61. Masood, M.T.; Qudsia, S.; Hadadian, M.; Weinberger, C.; Nyman, M.; Ahläng, C.; Dahlström, S.; Liu, M.; Vivo, P.; Österbacka, R.; et al. Investigation of Well-Defined Pinholes in TiO2 Electron Selective Layers Used in Planar Heterojunction Perovskite Solar Cells. *Nanomaterials* **2020**, *10*, 181. [CrossRef]
62. Zhao, C.; Zou, X.; He, S. $CdTeO_3$ deposited mesoporous NiO photocathode for a solar cell. *J. Nanomater.* **2014**, *2014*, 372381. [CrossRef]
63. Caballero-Briones, F.; Peña, J.L.; Martel, A.; Iribarren, A.; Zapata-Navarro, A. Structural analysis of Cd–Te–O films prepared by RF reactive sputtering. *J. Noncryst. Solids* **2008**, *354*, 3756–3761. [CrossRef]
64. Caballero-Briones, F.; Zapata-Navarro, A.; Martel, A.; Iribarren, A.; Peña, J.L.; Jiménez-Sandoval, S. Compositional mixture in RF sputtered CdTe oxide films. Raman spectroscopy results. *Superf. Vacio* **2003**, *16*, 38–42.
65. Carmona-Rodríguez, J.; Lozada-Morales, R.; Jiménez-Sandoval, O.; Rodríguez-Melgarejo, F.; Meléndez-Lira, M.; Jiménez-Sandoval, S.J. $CdTeO_x$ to $CdTeO_3$ structural phase transition in as-grown polycrystalline films by reactive sputtering. *J. Appl. Phys.* **2008**, *103*, 123516. [CrossRef]
66. Wu, L.; Li, Z.; Wang, D.; Lei, X.; Cai, Y.; Wang, D. CdTe surface passivation by electric field induced at the metal-oxide/CdTe interface. *Solar Energy* **2021**, *225*, 83–90. [CrossRef]
67. Erken, O. Effect of cycle numbers on the structural, linear and nonlinear optical properties in Fe_2O_3 thin films deposited by SILAR method. *Curr. Appl. Phys.* **2022**, *34*, 7–18. [CrossRef]
68. Sathya, M.; Selvan, G.; Karunakaran, M.; Kasirajan, K.; Usha, S.; Logitha, M.; Baskaran, P. Synthesis and characterization of cadmium doped on ZnO thin films prepared by SILAR method for photocatalytic degradation properties of MB under UV irradiation. *Eur. Phys. J. Plus* **2023**, *138*, 67. [CrossRef]
69. Lindroos, S.; Arnold, A.; Leskelä, M. Growth of CuS thin films by the successive ionic layer adsorption and reaction method. *Appl. Surf. Sci.* **2000**, *158*, 75–80. [CrossRef]
70. Menéndez-Proupin, E.; Giannozzi, P.; Peralta, J.; Gutiérrez, G. Ab initio molecular dynamics study of amorphous $CdTeO_x$ alloys: Structural properties. *Phys. Rev. B* **2009**, *79*, 014205. [CrossRef]
71. Weil, M. New phases in the Ca–Te–O and Cd–Te–O systems: Calcium tellurite (IV) $Ca_4Te_5O_{14}$ and the cadmium compounds $Cd2Te_3O_9$ and $Cd_2Te_2O_7$ with mixed-valent oxotellurium (IV/VI) anions. *Solid-State Sci.* **2004**, *6*, 29–37. [CrossRef]
72. Menéndez-Proupin, E.; Gutiérrez, G.; Palmero, E.; Peña, J.L. Electronic structure of binary and ternary components of CdTe:O thin films. *Phys. Status Solidi (C)* **2004**, *1*, S104–S107. [CrossRef]